nature materials

ARTICLES

PUBLISHED ONLINE: 24 MARCH 2013 | DOI: 10.1038/NMAT3580

Optical excitation of Josephson plasma solitons in a cuprate superconductor

A. Dienst[1], E. Casandruc[2], D. Fausti[1,2], L. Zhang[2], M. Eckstein[2], M. Hoffmann[2], V. Khanna[1,2], N. Dean[1], M. Gensch[3], S. Winnerl[3], W. Seidel[3], S. Pyon[4], T. Takayama[4], H. Takagi[4,5] and A. Cavalleri[1,2]*

Josephson plasma waves are linear electromagnetic modes that propagate along the planes of cuprate superconductors, sustained by interlayer tunnelling supercurrents. For strong electromagnetic fields, as the supercurrents approach the critical value, the electrodynamics become highly nonlinear. Josephson plasma solitons (JPSs) are breather excitations predicted in this regime, bound vortex–antivortex pairs that propagate coherently without dispersion. We experimentally demonstrate the excitation of a JPS in $La_{1.84}Sr_{0.16}CuO_4$, using intense narrowband radiation from an infrared free-electron laser tuned to the 2-THz Josephson plasma resonance. The JPS becomes observable as it causes a transparency window in the opaque spectral region immediately below the plasma resonance. Optical control of magnetic-flux-carrying solitons may lead to new applications in terahertz-frequency plasmonics, in information storage and transport and in the manipulation of high-T_c superconductivity.

Terahertz-frequency nonlinear optics holds great potential for device applications in data storage and manipulation at high bit rates, as well as for applications in the coherent control of matter. New tabletop and accelerator-based sources, which generate electric fields at megavolt per centimetre strengths, are opening up new opportunities in this area. Recent advances have relied on direct control of selected vibrational resonances[1–6] or on the use of field enhancement in metamaterial structures[7]. In cuprate superconductors, direct excitation of the order-parameter phase has been shown to modulate the superfluid density on the ultrafast timescale[8], effectively demonstrating non-dissipative routes to control the macroscopic state of the solid.

Here, the terahertz nonlinear optics of cuprate superconductors is studied experimentally and theoretically in the general case in which nonlinear propagation effects are combined with the local response of ref. 8. The intrinsic nonlinearity of interlayer tunnelling is shown to generate solitonic modes that concentrate the electromagnetic energy in space and time, propagating without distortion inside the material.

The terahertz-frequency electrodynamics of cuprate superconductors are, for fields polarized perpendicular to the planes, dominated by superconducting tunnelling between layers[9]. Cuprates are in fact stacks of extended Josephson junctions[10,11], with distributed tunnelling inductance $L_J(x,y,t)$ between capacitively coupled planes (x and y are the spatial coordinates in the planes and t is time).

For low fields, L_J is independent of space and time and a single Josephson plasma resonance (JPR) is found at $\omega_{JPR} = 2\pi/\sqrt{L_J C}$ (C is the equivalent capacitance of the planes, which is assumed to be constant in space and time). In most cuprates, ω_{JPR} ranges between gigahertz (refs 12,13) and terahertz (ref. 14) frequencies. As characteristic for a plasmonic response, the superconductor is transparent and frequency dispersive for $\omega > \omega_{JPR}$ and has unity reflectivity for $\omega < \omega_{JPR}$.

For high fields, the electrodynamics of the JPR become highly nonlinear[15,16]. As radiation at photon energies below the average superconducting gap does not strongly perturb the order-parameter amplitude (number of Cooper pairs) or the distribution of incoherent quasi-particles, the electrodynamics are primarily determined only by deformations of the space- and time-dependent order-parameter phase. The phase difference between adjacent layers (hereafter referred to only as phase φ_z) is the relevant parameter. From the Josephson equations, the phase $\varphi_z(x,y,t)$ advances in time as $\varphi_z(x,y,t) \propto \int E(x,y,t)\,dt$ and acts back onto the inductive coupling as $L_J(x,y,t) \propto 1/\cos\varphi_z(x,y,t)$. The resulting electrodynamics is well captured by the sine–Gordon equation[17], which in one dimension and in the absence of dissipation reads

$$\frac{\partial^2\varphi_z(x,t)}{\partial x^2} - \frac{\varepsilon_r}{c^2}\frac{\partial^2\varphi_z(x,t)}{\partial t^2} = \frac{1}{\lambda_J^2}\sin\varphi_z(x,t)$$

In this equation ε_r is the dielectric permittivity of the insulating layers, c is the speed of light in vacuum and λ_J is the Josephson penetration depth. For small electric fields and thus small phase, we have $\sin\varphi_z(x,t) \sim \varphi_z(x,t)$ and the sine–Gordon equation yields a linear wave equation, leading to Josephson plasma waves.

This equation also encapsulates most key phenomena observed in long or short Josephson junctions. If a static magnetic field is applied and the time dependence is neglected, for small fields the equation reduces to $\lambda_J^2(\partial^2\varphi_z/\partial x^2) = \varphi$, and thus predicts the Meissner effect $\varphi_z(x) = \varphi_z(0)\exp(-x/\lambda_J)$. For static magnetic fields that are large enough to prevent the small-phase approximation $\lambda_J^2(\partial^2\varphi/\partial x^2) = \sin\varphi$, which predicts a static Josephson vortex lattice with the phase advancing in steps of 2π with a periodicity of the Josephson penetration depth. Finally, if the junction is assumed to be short ($\ll\lambda_J$) and the spatial derivative is disregarded, $-\lambda_J^2(\varepsilon_r/c^2)(\partial^2\varphi/\partial t^2) = \sin\varphi$ and the equation predicts the conventional Josephson effect.

[1]Department of Physics, Clarendon Laboratory, University of Oxford, Oxford OX1 3PU, UK, [2]Max Planck Research Department for Structural Dynamics, University of Hamburg-CFEL, 22761 Hamburg, Germany, [3]Helmholtz-Zentrum Dresden-Rossendorf, 01328 Dresden, Germany, [4]Department of Advanced Materials Science, University of Tokyo, 113-8656 Tokyo, Japan, [5]RIKEN Advanced Science Institute, Hirosawa 2-1, Wako 351-0198, Japan.
*e-mail: andrea.cavalleri@mpsd.cfel.de.

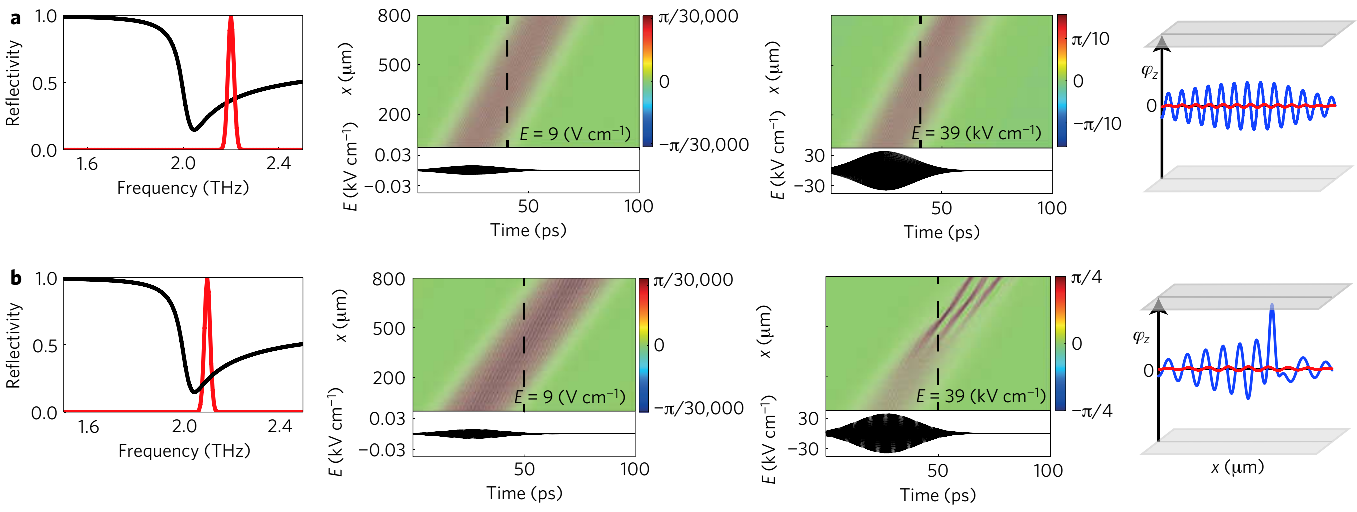

Figure 1 | Calculated space- and time-dependent interlayer phase for $\varphi_z(x,t)$ for two pump wavelengths above resonance. a, $\omega_{FEL}=1.1\omega_{JPR}$. **b**, $\omega_{FEL}=1.05\omega_{JPR}$. In the plots on the left, the pump spectrum is shown in red superimposed on the calculated broadband linear reflectivity of the cuprate. The phase $\varphi_z(x,t)$ is shown in the colour plots on the left for peak field strengths of $E=9\,\mathrm{V\,cm^{-1}}$ (linear excitation). The strong-field response for $E=39\,\mathrm{kV\,cm^{-1}}$ is plotted on the right in the colour plots and in the one-dimensional lineouts at 40 ps and 50 ps time delays for $\omega_{FEL}=1.1\omega_{JPR}$ and $\omega_{FEL}=1.05\omega_{JPR}$ respectively. The linear response is plotted in red.

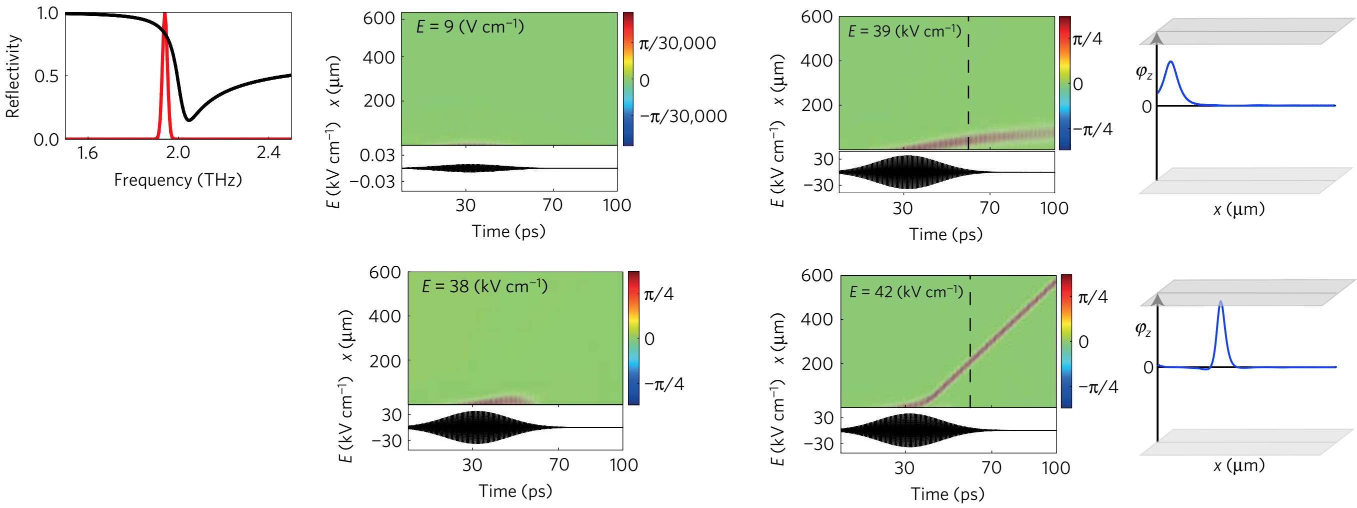

Figure 2 | Calculated space- and time-dependent interlayer phase for $\varphi_z(x,t)$ for $\omega_{FEL}=0.97\omega_{JPR}$ and four pump intensities: 9 V cm^{-1}, 38 kV cm^{-1}, 39 kV cm^{-1}, 42 kV cm^{-1}. In the plot on the left, the pump spectrum is shown in red superimposed on the calculated broadband linear reflectivity of the cuprate. The linear response in the colour plot on the left is for a peak field strength of $E=9\,\mathrm{V\,cm^{-1}}$. In the lower left graph a strong-field response is depicted for $E=38\,\mathrm{kV\,cm^{-1}}$, where a modified evanescent wave is excited but no propagating mode ensues. Two strong-field responses are plotted on the right in the one-dimensional lineouts for $E=39\,\mathrm{kV\,cm^{-1}}$ and $E=42\,\mathrm{kV\,cm^{-1}}$.

Here, the nonlinear optical properties of the optimally doped single-layer compound $La_{1.84}Sr_{0.16}CuO_4$ ($T_c=38$ K) are investigated theoretically and experimentally. We focus on the response near the 2-THz JPR, where the strongest nonlinearities are found.

We first present numerical solutions of the sine–Gordon equation, which will be shown to correctly predict the results of the experiments. The evolution of the space- and time-dependent order-parameter phase $\varphi_z(x,\tau)$ was calculated in this work by assuming that narrowband terahertz pulses impinged at normal incidence onto the superconducting cuprate, with electric fields polarized perpendicular to the planes. Details of these numerical simulations are discussed in the Methods.

In the colour plots of Fig. 1a,b, we show the calculated phase $\varphi_z(x,\tau)$ for excitation at two frequencies in the transparent region above the plasma resonance. We report results in the linear and nonlinear regime, that is, for 9 V cm^{-1} and 39 kV cm^{-1} peak fields. For excitation at $\omega_{FEL}=1.1\omega_{JPR}$ (Fig. 1a), a propagating mode is found with a group velocity $v_g=\partial\omega/\partial k=2.5\times10^7\,\mathrm{m\,s^{-1}}$, with little variation at higher field strength. Thus, for excitation frequencies far enough above ω_{JPR} the nonlinear response was found to be small.

The calculated response becomes strongly field dependent closer to resonance, for $\omega_{FEL}=1.05\omega_{JPR}$ (Fig. 1b). In the linear regime (9 V cm^{-1}), light propagates at $v_g=\partial\omega/\partial k=2\times10^7\,\mathrm{m\,s^{-1}}$, a slightly

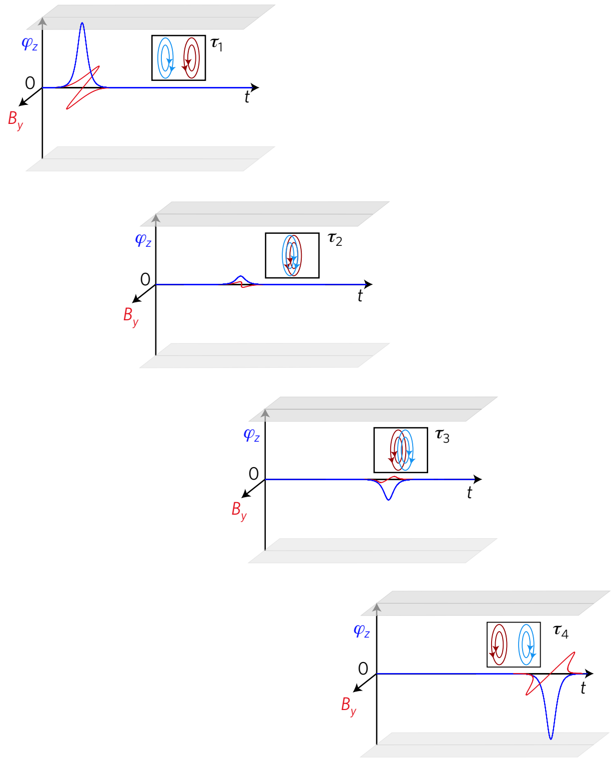

Figure 3 | Pictorial representation of a JPS as it propagates at four time delays. A bound kink–antikink pair (blue), with associated oppositely phased magnetic fields B_y, oriented along the y axis (red) oscillates as it propagates. The time spanned between τ_1 and τ_4 is half of a Josephson plasma period, corresponding to approximately 250 fs (not visible in Fig. 2). The equivalent representation in terms of an oscillating vortex–antivortex pair is included in the inset.

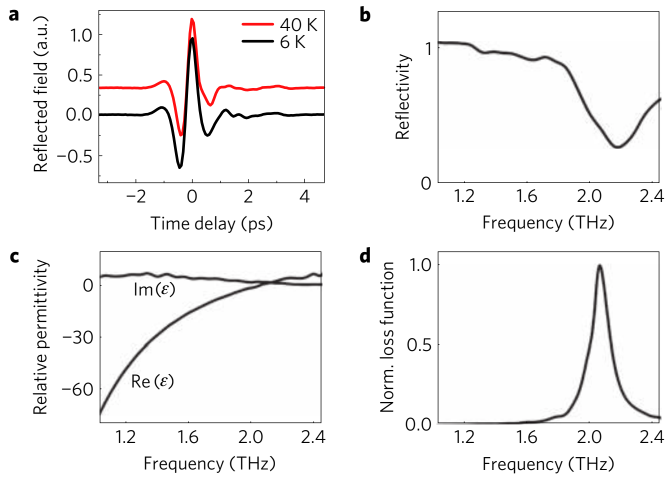

Figure 4 | Equilibrium optical properties of $La_{1.84}Sr_{0.16}CuO_4$. a, Reflected terahertz transients above (red) and below (black) $T_c = 36$ K. **b**, Intensity reflectivity $|r(\omega)|^2$ (black) in the frequency domain as extracted at 6 K from the time-resolved transients after normalization to the incident field. As the reflectivity relied on various calibrated parameters, it was known with only a few per cent accuracy, fluctuating around 1 for $\omega < \omega_{FEL}$. **c**, Real and imaginary part of the complex frequency-dependent permittivity $\varepsilon = \varepsilon_1 + i\varepsilon_2$ measured at 6 K. **d**, Normalized loss function at equilibrium $f(\omega)/f(\omega_J)$, with $f(\omega) = -\mathrm{Im}(1/\varepsilon(\omega))$, determined at 6 K.

lower group velocity than for $\omega_{FEL} = 1.1\omega_{JPR}$. In the strong-field regime, the phase profile is significantly perturbed, with sharpened and increased phase oscillation developing as the wave penetrates into the material, and with the pulse shape breaking up in a train.

The dynamics immediately below ω_{JPR}, shown in Fig. 2, is where the most interesting effects were obtained. For weak fields ($E = 9\,\mathrm{V\,cm^{-1}}$) the evanescent mode characteristic of linear excitation below a plasma resonance is observed, with screening occurring over a distance $1/\alpha = 18\,\mu$m. Strong deformation of the evanescent wave is obtained for $E = 38\,\mathrm{kV\,cm^{-1}}$. Remarkably, when the electric field exceeds a threshold of $39\,\mathrm{kV\,cm^{-1}}$ a propagating mode emerges. A spatial lineout of the phase for 60 ps time delay (upper right of the figure) shows a single solitonic pulse of amplitude $\varphi_z^{\mathrm{peak}}(x,\tau) \approx \pi/4$, which evolves from the exponentially evanescent wave at early times. These JPSs, excited for near-threshold electromagnetic field strengths, propagate at a small fraction of the speed of light ($v_g = 8 \times 10^5\,\mathrm{m\,s^{-1}}$, or $\sim 2.5 \times 10^{-3}\,c_0$). As the field strength is further increased to $42\,\mathrm{kV\,cm^{-1}}$ the pulse contracts further and speeds up, with a peak phase of $\varphi_z^{\mathrm{peak}}(x,\tau) \approx \pi/2$. At even higher fields (not shown here, see Supplementary Information), more than one soliton is launched during the pulse.

Figure 3 presents a caricature of a JPS, in which two self-localized[18–20] Josephson vortices propagate along the planes, oscillating against one another at a frequency determined by the strength of the binding. As a consequence, the peak of the phase pulse oscillates between positive and negative values. These excitations are also often referred to as breathers[21,22]. From the sine–Gordon equation, we estimate that the oscillation between positive and negative peak values occurs at a frequency $\nu_{OSC} \sim \nu_{JPR}$, thus with a period of only a few hundred femtoseconds (not visible in Fig. 2). We stress that size, peak value, propagation velocity and breathing frequency depend extremely sensitively on the excitation conditions. This field dependence is especially strong close to the $39\,\mathrm{kV\,cm^{-1}}$ threshold. We next turn to the experimental data, which validate the simulations discussed above.

First, we show the static, linear optical properties of unexcited bulk $La_{1.84}Sr_{0.16}CuO_4$ as measured in reflection at a 6 K base temperature by an ultrashort probe pulse with the electric field polarized perpendicular to the superconducting planes. These measurements are shown in Fig. 4. Single-cycle, broadband probe pulses, polarized along the c axis of the superconductor[23] were generated by a photoconductive antenna illuminated with a femtosecond laser[24]. The reflected pulses were measured by electro-optic sampling in ZnTe. In the superconducting state ($T < T_c = 38$ K), long-lived near-2-THz oscillations appeared on the trailing edge of the pulse (Fig. 4a, black trace). The frequency-dependent complex reflection coefficient was derived by Fourier transformation as $r(\omega) = E_{\mathrm{refl}}(\omega)/E_{\mathrm{inc}}(\omega)$. The incident electric field $E_{\mathrm{inc}}(\omega)$ was independently calibrated by using reflection at temperatures above T_c, where the reflectivity was featureless in this spectral range. The intensity reflectivity $|r(\omega)|^2$ is shown in Fig. 4b, and reproduces that found in numerous frequency-domain studies[25,26]. In Fig. 4c we report the complex permittivity $\varepsilon(\omega) = \varepsilon_1(\omega) + i\varepsilon_2(\omega)$ extracted from the reflectivity data[27]. The real part ε_1 is negative for frequencies below the plasma resonance, where the reflectivity nears 1. For $\omega > \omega_{JPR}$, ε_1 is positive and electromagnetic radiation can propagate inside the sample. The imaginary part ε_2 is small but finite over the whole frequency range, indicating weak dissipation by non-superconducting quasi-particles. In Fig. 4d, the loss function is shown, defined as $f(\omega) = -\mathrm{Im}[1/\varepsilon(\omega)]$. This function quantifies the amount of electromagnetic energy coupled into the Josephson plasma; it peaks at ω_{JPR} and exhibits Lorentzian line shape. The width is determined by damping. From the peak of the loss function we determine $\omega_{JPR} = 2.05$ THz.

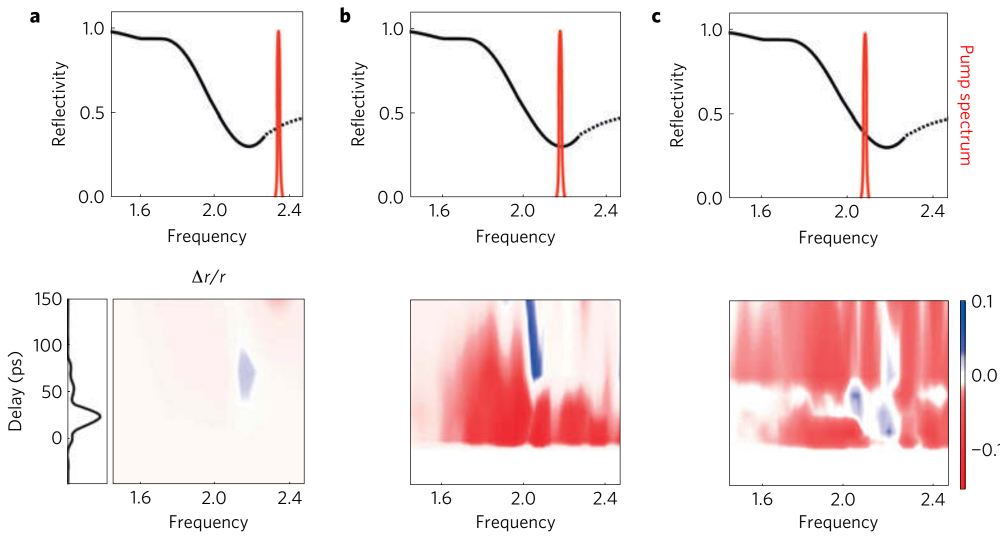

Figure 5 | Time-dependent optical properties of $La_{1.84}Sr_{0.16}CuO_4$ for three excitation frequencies. a–c, Top, the linear reflectivity of the sample over the whole broad bandwidth (black line). The pump spectrum is shown in red for the three conditions studied here $\omega_{FEL}=1.1\omega_{JPR}$, $\omega_{FEL}=1.05\omega_{JPR}$ and $\omega_{FEL}=\omega_{JPR}$. The time-dependent differential field reflectance $\Delta r(\omega,\tau)/r_0(\omega)$ is reported in the lower plots.

Figure 5 reports the pump–probe results. These experiments were uniquely made possible by the use of a terahertz free-electron laser (FEL), which emitted intense, narrowband ($\Delta\omega/\omega\sim 1\%$) pulses of 25-ps duration, and could be tuned around the 2-THz JPR. The excitations of the superconductor were then probed in the time domain using the same laser-generated, single-cycle terahertz pulses used to measure the static properties of Fig. 4. The laser oscillator was electronically synchronized to the FEL, and pump–probe time delays were scanned by offsetting the synchronization phase-locked loop and by an optical delay line for finer delays. The excitation by the FEL was tuned around the plasma resonance, at $\omega_{FEL}=1.1\omega_{JPR}$ (5a), $\omega_{FEL}=1.05\omega_{JPR}$ (5b) and $\omega_{FEL}\sim\omega_{JPR}$ (5c). The FEL wavelength was measured by using a grating spectrometer, which allowed for a precision better than 1%. Both pump and probe fields were polarized along the c axis, perpendicular to the superconducting planes. The pulse energy from the FEL was adjusted to 100 nJ and focused into spots of approximately 1 mm^2, resulting in peak fields of 10 kV cm^{-1} with a repetition rate of 13 MHz. Minimal heating resulted at this irradiation level, and the frequency of the JPR did not shift significantly on average. As the response of the system was probed at 78 MHz, only one pulse in six probed the light-induced dynamics. The data presented in the figure are derived from the experimental data with a factor of six linear scaling.

The colour plots in Fig. 5 show $\Delta r^{exp}(\omega,\tau)/r_0(\omega)$, relative changes in reflectance that are dependent on the frequency and the pump–probe time delay. For $\omega_{FEL}=1.1\omega_{JPR}$ (Fig. 5a) only small changes in the reflectivity were detected. For $\omega_{FEL}=1.05\omega_{JPR}$ (Fig. 5b) a decrease of reflectivity for $\omega>\omega_{FEL}$ and an increase over a narrow spectral window for $\omega<\omega_{FEL}$ was measured, indicative of a redshift of the edge. At $\omega_{FEL}\sim\omega_{JPR}$, the reflectivity data (Fig. 5c) show a drop in reflection at all frequencies, with a complex rearrangement in the optical properties.

Experiment and theory are compared in Fig. 6 for strong-field excitation. We discuss the results in terms of the time- and frequency- dependent loss function $f^{exp}(\omega,\tau)=-\mathrm{Im}(1/\varepsilon^{exp}(\omega,\tau))$, already introduced in Fig. 4d for the optical properties of the unperturbed superconductor. The experimental loss function was determined at each time delay by extracting the frequency-dependent dielectric constant $\varepsilon^{exp}(\omega,\tau)$ from the reflectance $r^{exp}(\omega,\tau)=r_0(\omega)+\Delta r^{exp}(\omega,\tau)$of Fig. 5. The reflectivity $r^{exp}(\omega,\tau)$ was fitted with a model that considered a surface layer (with thickness fixed to the pump wavelength penetration depth) of unknown properties over an unperturbed semi-infinite superconductor with the properties of Fig. 4. The frequency-dependent penetration depth of the probe pulses was included in this calculation.

The simulated strong-field phase profiles $\varphi_z(x,\tau)$ summarized in Figs 1 and 2 were used to calculate the expected time-dependent optical reflectivity $r^{calc}(\omega,\tau)$ (see Methods). The reflectivity was transformed into $\varepsilon^{calc}(\omega,\tau)$ by fitting it with the same model used for the experimental data.

Excellent agreement is found in Fig. 6 between theoretical and experimental loss functions for all of the above-resonance excitation wavelengths. The theory predicts a shift to the red of the loss function during the pump pulse and immediately thereafter, when the probed volume is being traversed by the nonlinear propagating plasma wave. No significant effect appears after the pump wave has propagated beyond the probe penetration depth. The effect is stronger as the pump wavelength is tuned closer to resonance. In the experiment, the resolution is not as sharp as in the simulations, and the redshift is clearly visible only for $\omega_{FEL}=1.05\omega_{JPR}$. This shift of the loss function is well understood from qualitative considerations. As the Josephson phase oscillates with large amplitude, the average inductance increases and, consequently, $\omega_{JPR}=2\pi/\sqrt{LC}$ decreases. These observations are an experimental confirmation for the self-induced transparency theoretically predicted in the literature for these experimental conditions[28].

Figure 6c compares the experimental and theoretical loss functions at $\omega_{FEL}\sim\omega_{JPR}$. During the pump pulse ($\tau<50$ ps), as the soliton is formed, the loss function is observed to broaden to the red. Owing to the extreme nonlinearity of this process, the reshaping of the loss function can be only qualitatively reproduced in the simulations.

At time delays after the excitation ($\tau>50$ ps), a long-lived dip is observed in both experiments and simulations. Lineouts for 80 ps time delay are compared in the uppermost plots of Fig. 6c. The split line shape with a dip is well understood by considering the optical properties of the solid in the presence of the JPS. As

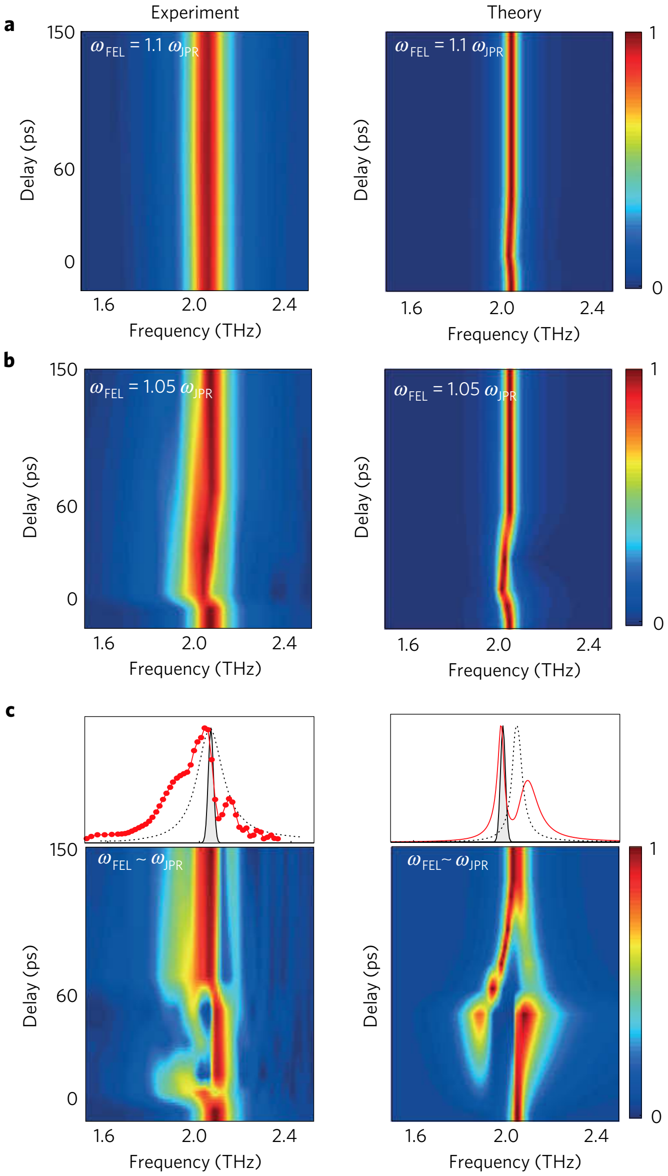

Figure 6 | Perturbed loss functions. a,b, Frequency- and time-delay-dependent loss function for $\omega_{FEL} = 1.1\omega_{JPR}$ (**a**) and $\omega_{FEL} = 1.05\omega_{JPR}$ (**b**). Experimental loss functions extracted from the data in Fig. 5 are shown on the left. The theoretical loss functions, extracted from the calculated high-field phase profiles of Fig. 1, are shown on the right. **c**, $\omega_{FEL} \sim \omega_{JPR}$. The experimental loss function, extracted from the reflectivity data in Fig. 5c, is shown on the left. The theoretical loss functions, extracted from the calculated high-field phase profiles of Fig. 2, that is, for a field strength of 39 kV cm^{-1}, are shown on the right. At time delays larger than 50 ps both lineouts exhibit a splitting of the loss function. The lineouts shown in the uppermost part of the figure report the unperturbed loss function (black dotted line), the perturbed loss function at 80 ps time delay (red curve) and a Gaussian fit to the pump spectrum (black, shaded). The best fit is obtained for simulations at $\omega_{FEL} \sim 0.97\omega_{JPR}$ (see text).

the probe interrogates the superconductor, the optical response becomes determined by the superposition of regions in which the JPS is present ($\varphi_z(x,t) \gg 0$) and regions for which $\varphi_z(x,t) \sim 0$. Interference occurs throughout the spectrum. One useful analogy for the split line shape is with the effect of anharmonically coupled plasmon excitations in metallic micro-structures[29], where the optical response of a linear plasma mode is reshaped in a similar manner. One can also draw a parallel with physical systems in which continuum excitations are anharmonically coupled to discrete ones, such as in the Fano effect[30] or in electromagnetically induced transparency[31,32].

We note that the line shape observed in the experiment here could not be explained by incoherent quasi-particle excitations. This is well understood by considering that in the sine–Gordon equation quasi-particle damping is accounted for by the term $\gamma(\partial\varphi_z(x,t)/\partial t)$, where γ is the scattering time between the phase and quasi-particles. Quasi-particle excitations then act only to broaden the linewidth.

In the simulated plots, the dip decays on a timescale that matches the escape time of the soliton from the probe volume (5–20 μm depending on the wavelength). The calculated decay time of the dip for $E = 39$ kV cm^{-1} is 40 ps, as opposed to the measured value of 150 ps. This indicates that our simulations overestimate the velocity of the breather by a factor of 3–4. We recall that the simulations consider only a single junction without disorder. The discrepancy in velocity may be qualitatively explained by the fact that disorder may cause the soliton to slow down further from the ideal case.

Two further quantitative differences are to be found between theory and experiment. First, the calculations predict the formation of a slow soliton (thus causing a long-lived dip) when the excitation field is approximately 40 kV cm^{-1}, a factor of 3 or 4 above the experimentally determined value of 10 kV cm^{-1}. Various effects may lead to more efficient coupling of the light in the experiment, including the physics of a stack of junctions (not considered in the simulations), which may amplify the nonlinearity. Furthermore, our experiments are nominally performed at pump frequencies of $\omega_{FEL} \sim \omega_{JPR}$, but are best described by calculations performed at $\omega_{FEL} = 0.97\omega_{JPR}$. We note that the confidence level on the relative calibration of the pump wavelength and the probe is approximately 1% (the pump wavelength is measured with a grating spectrometer as opposed to time-delay terahertz detection for the probe pulses). This difference seems then to be significant. However, as the experimental linewidth is broader than the one obtained in the simulations, it is quite possible that inhomogeneous (caused by disorder) broadening may be at play in the experiment. A more complex spectral reshaping is in fact observed, including broadening to the red of the perturbed experimental loss function.

We reported a theoretical and experimental study of terahertz nonlinear optics of Josephson plasma excitations in superconducting cuprates. For excitation above the plasma resonance our experiments confirm the optical effects predicted in previous theoretical work[1,2], causing transparency through a light-induced shift of the resonance. For excitation at the plasma resonance, a slowly propagating mode is excited, which our simulations identify as a JPS. As a result, a transparency window caused by interference is created, reminiscent of effects observed in plasmonic metamaterials[27]. Various applications to plasmonics[33], as well as new strategies for optical control of superconductivity, can be predicted from our work. We recall that the control of flux-carrying phase kinks has been considered in conventional Josephson junctions for information transport and storage[34,35], for which currents were used as a means to control a fluxon shift register. Here, we demonstrate how such flux carriers can be driven and detected by light. Combining these ideas with terahertz coherent control techniques[36] may open up many new opportunities. Light could be here used to generate, stop, accelerate or slow down flux-carrying JPSs. Further, the control of JPS may be used for sensing of static vortices, or even to pin, de-pin, anneal or move vortices in the presence of static magnetic fields.

Methods

Simulation of the nonlinear optical properties from the sine–Gordon equation. We consider a stack of Josephson junctions with semi-infinite layers stacked along the z direction. A free surface at $x=0$ is considered, where optical pump and probe pulses, with the electrical field vector along z, impinge at normal incidence and propagate along x. We assume translational invariance in the y direction, and the propagation of the Josephson phase difference across each layer of the cuprate is described by a one-dimensional sine–Gordon equation

$$\frac{\partial^2\varphi}{\partial x^2}-\frac{\varepsilon}{c^2}\frac{\partial^2\varphi}{\partial t^2}=\frac{1}{\lambda_J^2}\sin\varphi \tag{1}$$

Tangential components of both the electric and magnetic fields are made continuous at the boundary between the vacuum and the superconductor. The following boundary conditions for the phase are used

$$[E_i(t)+E_r(t)]_{x=-0}=E_c(x,t)|_{x=+0}=H_0\frac{1}{\omega_{JPR}\sqrt{\varepsilon}}\left.\frac{\partial\varphi(x,t)}{\partial t}\right|_{x=+0} \tag{2}$$

$$[H_i(t)+H_r(t)]_{x=-0}=H_c(x,t)|_{x=+0}=-H_0\lambda_J\left.\frac{\partial\varphi(x,t)}{\partial x}\right|_{x=+0} \tag{3}$$

The subscripts i, r and c stand for fields impinging, reflected and propagating inside the cuprate. In this expression, $H_0=\Phi_0/2\pi D\lambda_J$, where Φ_0 is the flux quantum and D is the distance between adjacent superconducting layers. For these equations, the value of the plasma resonance is chosen to be $\omega_{JPR}=2.05$ THz. The damping time was extracted from a fit to the data reported in Fig. 1.

For fields in vacuum ($x<0$), Maxwell's equations imply

$$E_i-E_r=\frac{\omega\mu}{ck}(H_i+H_r)=H_i+H_r \tag{4}$$

Combining equation (4) with equations (2) and (3), we can calculate the propagation of the Josephson phase by solving the sine–Gordon equation with one boundary condition

$$\frac{2\sqrt{\varepsilon}}{H_0}E_i(t)|_{x=-0}=\left.\frac{\partial\varphi(x,t)}{\omega_{JPR}\partial t}\right|_{x=+0}-\sqrt{\varepsilon}\left.\frac{\partial\varphi(x,t)}{\partial x/\lambda_J}\right|_{x=+0} \tag{5}$$

and then obtain the reflected field from equation (2). The static reflectivity of the cuprate is obtained by computing the ratio between the Fourier transforms of the reflected field and a weak input field

$$r^{\text{static}}(\omega)=E_r^{\text{static}}(\omega)/E_i(\omega) \tag{6}$$

Permittivity, conductivity and loss can be calculated from $r^{\text{static}}(\omega)$. In the simulation, we renormalize the input field as $E_i'(t)=2\sqrt{\varepsilon}E_i(t)/H_0$. $E_i'=1$ corresponds to $E_i\approx 30\,\text{kV cm}^{-1}$.

For the pump–probe configuration, the input field is the sum of the pump field and the probe field (note that there may be a delay between them)

$$E_i(t)=E_{\text{pump}}(t)+E_{\text{probe}}(t) \tag{7}$$

Correspondingly, the Josephson phase can be decomposed as

$$\varphi=\varphi_{\text{pump}}+\varphi_{\text{probe}} \tag{8}$$

Substituting this equation into the sine–Gordon equation equation (1) and using the relation $\sin(\varphi_{\text{pump}}+\varphi_{\text{probe}})=\sin\varphi_{\text{pump}}\cos\varphi_{\text{probe}}+\cos\varphi_{\text{pump}}\sin\varphi_{\text{probe}}$, we obtain two coupled equations

$$\frac{\partial^2\varphi_{\text{pump}}}{\partial x^2}-\frac{\varepsilon}{c^2}\frac{\partial^2\varphi_{\text{pump}}}{\partial t^2}=\frac{1}{\lambda_J^2}\sin\varphi_{\text{pump}}\cos\varphi_{\text{probe}} \tag{9}$$

$$\frac{\partial^2\varphi_{\text{probe}}}{\partial x^2}-\frac{\varepsilon}{c^2}\frac{\partial^2\varphi_{\text{probe}}}{\partial t^2}=\frac{1}{\lambda_J^2}\sin\varphi_{\text{probe}}\cos\varphi_{\text{pump}} \tag{10}$$

For a weak probe ($\varphi\ll 1$), $\cos\varphi_{\text{probe}}\approx 1$ and the effect of φ_{probe} on φ_{pump} can be neglected in equation (9). The simulation can then be performed in two steps: solve equations (9) and (5) with the driving field $E_i=E_{\text{pump}}$ to get $\varphi_{\text{pump}}(x,t)$ (the spatial-temporal propagation of breathers); substitute $\varphi_{\text{pump}}(x,t)$ into equation (10) and solve this equation together with equation (5) with the driving field $E_i=E_{\text{probe}}$, which will give us $\varphi_{\text{probe}}(x,t)$ and the reflected probe field E_r^{perturb}. The perturbed reflectivity is given by

$$r^{\text{perturb}}(\omega)=E_r^{\text{perturb}}(\omega)/E_i(\omega) \tag{11}$$

Once r^{perturb} is calculated, it is compared with the experimental results by fitting with a model that considers a surface layer (with a depth fixed to the pump wavelength penetration depth) over an unperturbed semi-infinite superconductor with the optical properties calculated from equation (4).

Received 24 October 2011; accepted 28 January 2013; published online 24 March 2013

References

1. Rini, M. *et al.* Control of the electronic phase of a manganite by mode-selective vibrational excitation. *Nature* **449,** 72–74 (2007).
2. Tobey, R. I., Prabhakaran, D., Boothroyd, A. T. & Cavalleri, A. Ultrafast electronic phase transition in $La_{1/2}Sr_{3/2}MnO_4$ by coherent vibrational excitation: Evidence for nonthermal melting of orbital order. *Phys. Rev. Lett.* **101,** 197404 (2008).
3. Caviglia, A. D. *et al.* Ultrafast strain engineering in complex oxide heterostructures. *Phys. Rev. Lett.* **108,** 136801 (2012).
4. Fausti, D. *et al.* Light-induced superconductivity in a stripe-ordered cuprate. *Science* **331,** 189–191 (2011).
5. Först, M. *et al.* Nonlinear phononics as an ultrafast route to lattice control. *Nature Phys.* **7,** 854 (2011).
6. Först, M. *et al.* Driving magnetic order in a manganite by ultrafast lattice excitation. *Phys. Rev. B* **84,** 241104(R) (2011).
7. Liu, M. *et al.* THz field induced insulator to metal transition in vanadium dioxide metamaterial. *Nature* **487,** 345–348 (2012).
8. Dienst, A. *et al.* Bi-directional ultrafast electric-field gating of interlayer charge transport in a cuprate superconductor. *Nature Photon.* **5,** 485–488 (2011).
9. Lawrence, W. E. & Doniach, S. in *Proc. 12th Int. Conf. Low Temp. Phys.* (ed. Kanda, E.) 361–362 (Tokyo Keigaku Publishing, 1971).
10. Kleiner, R., Steinmeyer, F., Kunkel, G. & Muller, P. Intrinsic Josephson effects in $Bi_2Sr_2CaCu_2O_8$ single-crystals. *Phys. Rev. Lett.* **68,** 2394–2397 (1992).
11. Tsui, O. K. C., Ong, N. P., Matsuda, Y., Yan, Y. F. & Peterson, J. B. Sharp magnetoabsorption resonances in the vortex state of $Bi_2Sr_2CaCu_2O_{8+\delta}$. *Phys. Rev. Lett.* **73,** 724–727 (1994).
12. Matsuda, Y., Gaifullin, M. B., Kumagai, K., Kadowaki, K. & Mochiku, T. Collective Josephson plasma resonance in the vortex state of $Bi_2Sr_2CaCu_2O_{8+\delta}$. *Phys. Rev. Lett.* **75,** 4512–4515 (1995).
13. Tsui, O. K. C., Ong, N. P. & Peterson, J. B. Excitation of the Josephson plasma mode in $Bi_2Sr_2CaCu_2O_{8+\delta}$ in an oblique field. *Phys. Rev. Lett.* **76,** 819–822 (1996).
14. Tamasaku, K., Nakamura, Y. & Uchida, S. Charge dynamics across the CuO_2 planes in $La_{2-x}Sr_xCuO_4$. *Phys. Rev. Lett.* **69,** 1455–1458 (1992).
15. Savel'ev, S., Rakhmanov, A. L., Yampol'skii, V. A. & Nori, F. Analogues of nonlinear optics using terahertz Josephson plasma waves in layered superconductors. *Nature Phys.* **2,** 521–525 (2006).
16. Savel'ev, S., Yampol'skii, V. A., Rakhmanov, A. L. & Nori, F. Terahertz Josephson plasma waves in layered superconductors: Spectrum, generation, nonlinear and quantum phenomena. *Rep. Prog. Phys.* **73,** 026501 (2010).
17. Hu, X. & Lin, S. Z. Phase dynamics in a stack of inductively coupled intrinsic Josephson junctions and terahertz electromagnetic radiation. *Supercond. Sci. Technol.* **23,** 053001 (2010).
18. Sievers, A. J. & Takeno, S. Intrinsic localized modes in anharmonic crystals. *Phys. Rev. Lett.* **61,** 970–973 (1988).
19. Trombettoni, A. & Smerzi, A. Discrete solitons and breathers with dilute Bose–Einstein condensates. *Phys. Rev. Lett.* **86,** 2353–2356 (2001).
20. Sharon, E., Cohen, G. & Fineberg, J. Propagating solitary waves along a rapidly moving crack front. *Nature* **410,** 68–71 (2001).
21. Flach, S. & Willis, C. R. Discrete breathers. *Phys. Rep.* **295,** 181–264 (1998).
22. Vitanov, N. K. Breather and soliton wave families for the sine-Gordon equation. *Proc. R. Soc. Lond. A* **454,** 2409–2423 (1998).
23. Thorsmolle, V. K. *et al.* C-axis Josephson plasma resonance observed in $Ti_2Ba_2CaCu_2O_8$ superconducting thin films by use of terahertz time-domain spectroscopy. *Opt. Lett.* **26,** 1292–1294 (2001).
24. Dreyhaupt, A., Winnerl, S., Dekorsy, T. & Helm, M. High-intensity terahertz radiation from a microstructured large-area photoconductor. *Appl. Phys. Lett.* **86,** 121114 (2005).
25. Kresin, V. Z. & Morawitz, H. Layer plasmons and high-T_c superconductivity. *Phys. Rev. B* **37,** 7854–7857 (1988).
26. Basov, D. N. *et al.* Sum rules and interlayer conductivity of high-T_c cuprates. *Science* **283,** 49–52 (1999).
27. Dordevic, S. V., Komiya, S., Ando, Y. & Basov, D. N. Josephson plasmon and inhomogeneous superconducting state in $La_{2-x}Sr_xCuO_4$. *Phys. Rev. Lett.* **91,** 167401 (2003).
28. Apostolov, S. S., Maizelis, Z. A., Sorokina, M. A., Yampol'skii, V. A. & Nori, F. Self-induced tunable transparency in layered superconductors. *Phys. Rev. B* **82,** 144521 (2010).
29. Liu, N. *et al.* Plasmonic analogue of electromagnetically induced transparency at the Drude damping limit. *Nature Mater.* **8,** 758–762 (2009).
30. Fano, U. Effects of configuration interaction on intensities and phase shifts. *Phys. Rev.* **124,** 1866–1878 (1961).

31. Boller, K-J., Imamoglu, A. & Harris, S. E. Observation of electromagnetically induced transparency. *Phys. Rev. Lett.* **66,** 2593–2596 (1991).
32. Abdumalikov, A. A. Jr *et al.* Electromagnetically induced transparency on a single artificial atom. *Phys. Rev. Lett.* **104,** 193601 (2010).
33. Ozyuzer, L. *et al.* Emission of coherent THz radiation from superconductors. *Science* **318,** 1291–1293 (2007).
34. Fulton, T. A., Dynes, R. C. & Anderson, P. W. Flux shuttle-Josephson junction shift register employing single flux quanta. *Proc. IEEE* **61,** 28–35 (1973).
35. Nakajima, K., Onodera, Y. & Ogawa, Y. Logic design of Josephson network. *J. Appl. Phys.* **47,** 1620–1627 (1976).
36. Feurer, T. A., Vaughan, J. C. & Nelson, K. A. Spatiotemporal control of lattice vibrational waves. *Science* **413,** 374–377 (2001).

Acknowledgements

We thank Y. Laplace for fruitful discussions. Research at the University of Oxford was supported by a 2004 European Young Investigator Award, by the Royal Society through the Paul Instrument Fund and by the EPSRC under the program Next Generation Facility Users. Research at the MPSD-CFEL in Hamburg was funded through core support by the Max Planck Society and the University of Hamburg. E.C. acknowledges the support from IMPRS-UFAST. We are grateful to P. Michel and the FELBE team for their dedicated support.

Author contributions

A.C. conceived the project. A.D. and D.F. designed and built the experimental set-up and led the experimental activities. A.D., D.F., M.H., V.K. and N.D. performed the experiment and collected the data with assistance from M.G., S.W. and W.S.; A.D. analysed the data. E.C., L.Z. and M.E. developed the theoretical model and performed the simulation. S.P., H.T. and T.T. grew the samples. A.C. wrote the manuscript with contributions from E.C., L.Z. and M.E.

Additional information

Supplementary information is available in the online version of the paper. Reprints and permissions information is available online at www.nature.com/reprints. Correspondence and requests for materials should be addressed to A.C.

Competing financial interests

The authors declare no competing financial interests.